Journal of Constructional Steel Research 109 (2015) 34–46

Contents lists available at ScienceDirect

Journal of Constructional Steel Research

An innovative seismic performance enhancement technique for steel building moment resisting connections

Machel Morrison, Doug Schweizer [1], Tasnim Hassan *

Department of Civil, Construction and Environmental Engineering, North Carolina State University, Raleigh, NC 27607, United States

ARTICLE INFO

Article history:
Received 25 July 2014
Accepted 26 February 2015
Available online xxxx

Keywords:
Steel moment connection
Seismic performance enhancement
Beam plastic hinge
Heat-treated beam section
Reduced beam section

ABSTRACT

This study develops and experimentally validates an innovative technique for enhancing the seismic performance of steel beam to column moment connections. The technique involves reducing the strength of specified regions of the beam flanges by exposing them to high temperatures followed by slow cooling. Analogous to the reduced beam section (RBS) connection, yielding and plastic hinge formation is promoted in the heat-treated beam section (HBS). Moreover, because the elastic and inelastic modulus of the steel is unmodified by the heat-treatment and the beam cross section is not altered, an HBS connection does not sacrifice elastic stiffness or buckling resistance as does the RBS. Design of the HBS connection was performed through detailed finite element analysis and material testing. Two large scale connections modified with the HBS technique were tested in this study. The test program showed that the proposed heat-treatment technique was successful in the promotion of yielding and plastic hinge development in the heat-treated regions with specimens attaining interstory drifts as high as 6% without weld or near weld fracture. Strength degradation due to beam buckling within the HBS was the observed failure mechanism in both specimens. Detail analyses of strain and beam deformation data are presented to explain the HBS connection plastic hinge formation and gradual strength degradation. Broader applications of the technique to other structural components are identified.

1. Overview of steel moment connection advances since Northridge earthquake

Extensive damage to steel moment resisting frame connections during the 1994 Northridge earthquake instigated a comprehensive research effort led by the SAC joint venture intended to develop a broad and fundamental understanding of the seismic performance of moment frame connections [1]. A multitude of failure modes were observed in moment connections following the earthquake, the most common of which were fractures originating at or near the beam flange CJP welds which accounted for approximately 80% of the damage to welded steel moment frames [2]. In many cases these fractures propagated to other areas of the connection for example, column flanges, column web and beam web [3].

Initially, poor quality welds stemming from improper workmanship, use of welding electrodes which deposit weld metal with inherently low toughness, and a lack of careful inspection practice were thought to be the main causes for these brittle failures. However, studies that incorporated weld fracture mitigation measures alone showed that improvements in welding, inspection practice and weld metal are insufficient to guarantee adequate performance of these connections in high seismic areas [4–6]. One of these studies, performed by Stojadinovic et al. [4], evaluated the welded unreinforced flange-bolted web connection (WUF-B), which was one of the most commonly used moment resisting connections (prior to Northridge) due to their perceived ductility and economy [7,8]. As a part of the study, moment connections were fabricated to pre-Northridge standards and tested to in an effort to recreate the brittle failures discovered after Northridge and in doing so confirm the reasons for these failures. Subsequently, connections fabricated using "notch tough" weld metal, improved welding procedure, improved welding inspection and more careful connection detailing were evaluated. The study showed the pre-Northridge connections to be brittle as was also shown by Engelhardt and Husain [9] and Popov et al. [3]. The WUF-B connections exhibited little to no ductility with fractures emanating from the beam flange to column flange CJP weld root or toe and propagating along different paths. Among the failures were divot pull outs of the weld and column flange material, crack propagation through the column flange and web, crack propagation through the beam web, beam flange gross section fractures at the weld toe and weld root [4].

The so called 'SAC post-Northridge' connections tested by Stojadinovic et al. [4] displayed improved performance, however none of these connections were able to attain the required 0.03 radians plastic rotation in the standard proof test defined in the FEMA interim guidelines and the 1997 AISC Seismic provisions for steel buildings [4]. Careful examination of these connections through experimental and analytical studies,

* Corresponding author. Tel.: +1 919 515 8123.
E-mail address: thassan@ncsu.edu (T. Hassan).
[1] Currently at Thornton Tomasetti, Washington, DC.

http://dx.doi.org/10.1016/j.jcsr.2015.02.010
0143-974X/

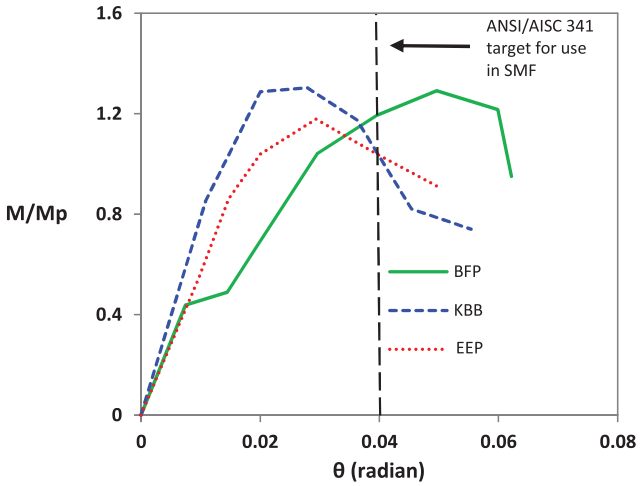

Specimen	Failure Mechanism
BFP (Specimen 7 Schneider and Teeraparbwong [16])	Fracture of beam flange in region of severe local buckling
KBB (Specimen 8 Adan and Gibb [14])	Fracture of beam flange in region of severe local buckling
EEP (8 bolt stiffened extended end plate. Specimen 8ES-1.25-1.75-30 - Murray et al [12])	Test stopped due to lateral instability of beam

Fig. 1. Moment-rotation experimental backbone curves (in positive bending) of stiffened connections.

suggested that beam flanges were "overstressed" due to stress redistribution and stress risers imposed by the configuration of the connection which ultimately limited connection plastic rotation capacity [10]. However, a study conducted by Xue et al. [11] showed evidence, albeit with a limited number of tests, that weld fracture mitigation strategies combined with a fully welded beam web could produce plastic rotations larger than 0.03 rads. Nonetheless, Stojadinovic et al. [4] concluded that weld fracture mitigation strategies alone are insufficient and that in future, moment connections intended for use in special moment frames (SMF) should incorporate both "weld mitigation measures as well as overstress mitigation measures". As such, many subsequent research studies focused on lowering these stress and strain demands through various means. The fundamental change in the design philosophy of these moment connections to that of the pre-Northridge connection is the development of a plastic hinge away from the beam end intended to act as a reliable and ductile seismic fuse. In most of these connections the relocation of the plastic hinge is accomplished through strengthening and stiffening the connection by adding endplates with stiffeners [12], cover plates [13], castings [14], haunches [15] etc. to encourage plastic hinging in the beam just beyond the strengthened region. The intent being that the strengthened connection would primarily remain elastic while plastic hinging of the beam takes place, thereby reducing the plastic strain demands and stress concentrations in the critical connection region.

Studies conducted by Sumner and Murray [12] demonstrated the use of extended end plate (EEP) connections with and without stiffeners to enhance the ductility of moment connections. Schneider and Teeraparbwong [16] and Sato et al. [17] demonstrated that carefully designed bolted flange plate (BFP) connections were successful in causing hinging of the beam section beyond the flange plate and that this led to a ductile and reliable failure mechanism. Adan and Gibb [14] evaluated proprietary cast high strength steel "Kaiser" bolted brackets (KBB) which were either bolted or welded to the beam flange and then bolted to the column flange. In this study it was demonstrated that similar to stiffened extended end plate and bolted flange plate connections the KBB strengthens the beam column connection region and forces plastic hinging, buckling and eventually fracture of the beam flange just beyond the end of the bracket.

Fig. 1 shows experimental backbone curves for selected EEP, BFP and KBB connections from these studies. Moments have been normalized based on plastic moment capacities reported in the respective studies. Both moments and rotations were computed with respect to the column centerline. Note in Fig. 1 that all these connections were successful in achieving their plastic moment capacity and exceeded the 2010 ANSI/AISC 341 Seismic Provisions [18] performance criteria for use in SMF's. As a result, they are now included in the 2010 ANSI/AISC 358 Prequalified Connections for Special and Intermediate Moment

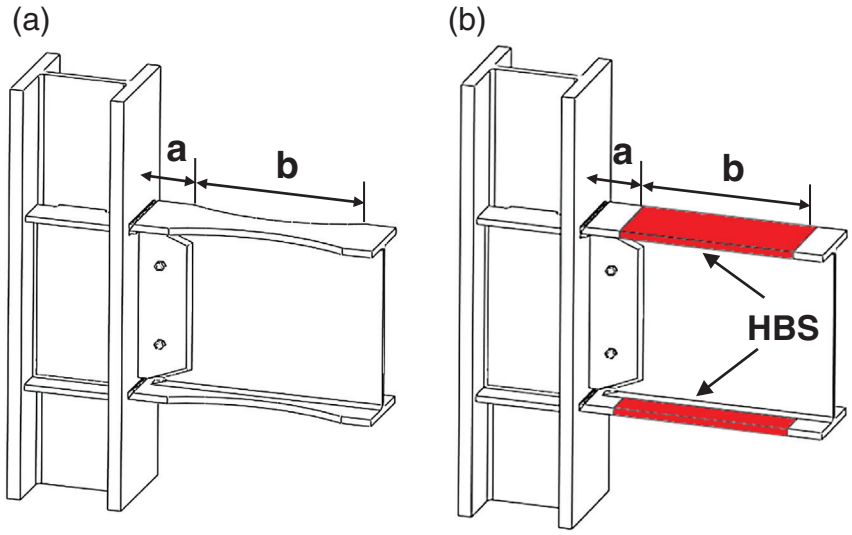

Fig. 2. Sketch of (a) reduced beam section (RBS) and (b) heat-treated beam section (HBS).

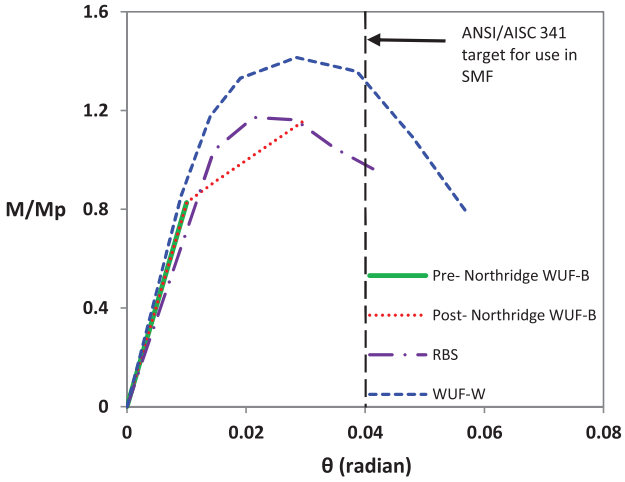

Specimen	Failure Mechanism
Pre Northridge WUF-B (Specimen 1.2 Standojvic et al. [30])	Column Divot pull out fracture
Post Northridge WUF-B (Specimen 7.2 Standojvic et al. [30])	Beam flange fracture in HAZ (Post-Northridge WUF-B)
RBS (Specimen DB3 Engelhardt et al. [22])	Test stopped due to lateral instability of beam
WUF-W (Specimen T5 Ricles et al. [6])	Fracture of beam flange in region of severe local buckling

Fig. 3. Moment-rotation experimental backbone curves (in positive bending) of welded unreinforced connections.

Frames for Seismic Applications [19]. It is also important to note that in the case of the BFP and to a lesser extent the KBB, plastic rotation is achieved through various mechanisms, for example beam flange and web yielding, panel zone yielding, small amounts of flange plate or Kaiser Bracket yielding and slip of beam flange and column flange bolts. This slip produces pinching of the hysteresis curves which can be identified in the backbone curve for the BFP connection by a reduction in stiffness at a rotation angle of about 0.01 rad followed by an increase of stiffness at approximately 0.015 rad. Slip can be a favorable energy dissipation mechanism but if excessive, p-δ effects may become significant due to large interstory drifts. Therefore, careful design and detailing of bolt holes is important to allow for both ease of field erection and preventing excessive rotations from slip. Note also that some of these strengthened connections displayed a variety of failure modes in laboratory experiments [14,16]. As a result, in some cases limit state design may be tedious and the predictability of failure mechanisms is questionable.

Another 'overstress' mitigation technique is to weaken the beam adjacent to the connection so as to create a fuse for damage and energy dissipation in this weakened region. The reduced beam section (RBS) shown in Fig. 2a employs such a strategy and has been widely tested and adopted in the ANSI/AISC 358 [19]. When combined with an all welded connection (welded flange and web) the RBS successfully develops plastic hinging of the beam in the reduced section and as a result relives the high inelastic strain demands at the beam flange groove welds, thereby reducing the likelihood of weld or near weld failures [20]. Experimental studies by Plumier [21], Engelhardt et al. [22], Chi and Uang [23] along with several others have demonstrated this improved ductility.

A consequence of the flange area reductions is the decrease in the elastic stiffness of frames employing such connections and as such, increases in maximum interstory drifts when subjected to lateral loads. Kim and Engelhardt [24] reported that flange reductions between 40% and 50% resulted in increased story drifts of 4.5% to 8%. In design practice this problem is suitably overcome by the use of larger beam sizes than would otherwise be necessary. An advantage of the RBS is that the flange width reduction may delay local flange buckling, but the consequential disadvantage is that the reduced flange stiffness lowers resistance to local web buckling and lateral torsional buckling [7]. However strength degradation associated with this reduced buckling resistance has been shown to be delayed in RBS connections tested with concrete slabs [25] and in bare steel connections with lateral bracing at the reduced section [26]. Despite these drawbacks the RBS is widely considered to provide an attractive combination of performance, economy and simplicity (both in design and construction) when compared to strengthened connections, making it one of the most widely used connections in SMF's.

Studies conducted by Ricles et al. [6] and Lee et al. [27] showed that welded unreinforced flange-welded web connections (WUF-W) which combine the use of fracture tough weld metal, a modified access hole design, a CJP welded web and reinforcing filet welds between the beam web and the shear tab could also successfully meet the

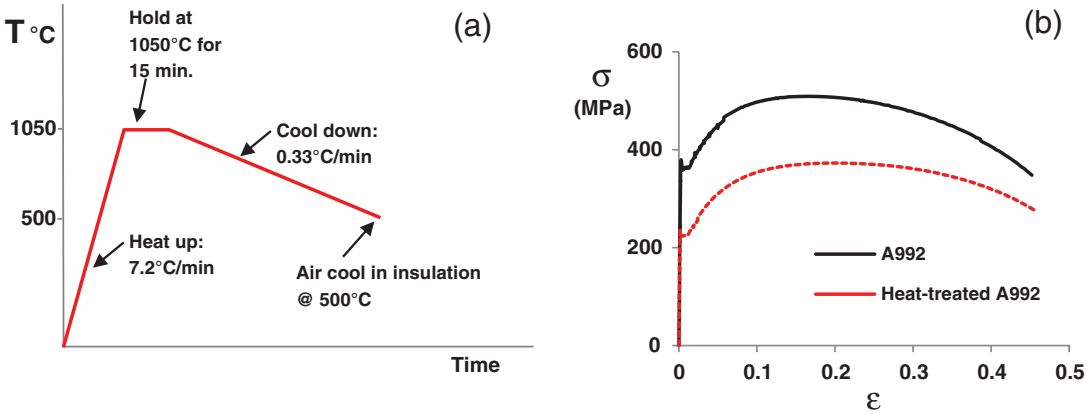

Fig. 4. (a) Temperature history of A992 heat-treatment. (b) Engineering stress–strain response of A992 and heat-treated A992 steel.

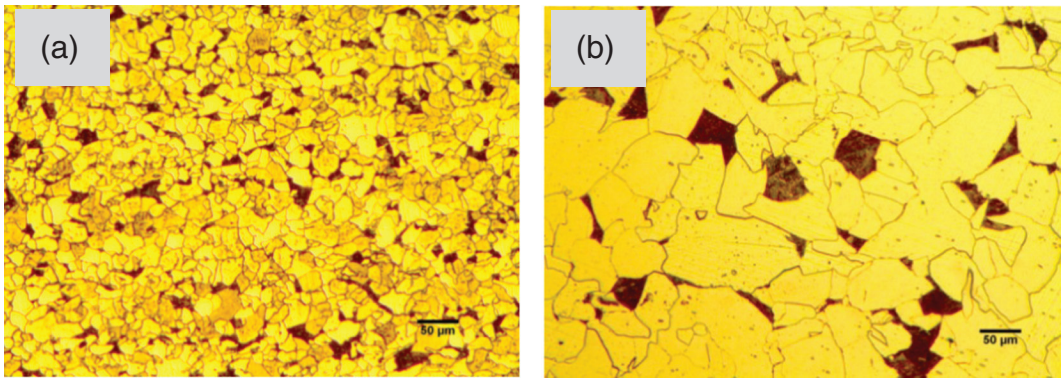

Fig. 5. Optical micro graphs of A992 Steel (a) before heat-treatment and (b) after heat-treatment at 1050 °C cooled at 20 °C/h to 500 °C followed by air cooling. Nital etch. Original magnification: 100×.

aforementioned AISC performance criteria. It is noted that the WUF-W makes use of a stiffened web connection which in effect redirects stresses away from the beam flanges. This concept was previously validated on free flange moment connections by Choi et al. [28]. The WUF-W has also been prequalified in the 2010 ANSI/AISC 358 [19] for use in SMFs. Fig. 3 shows experimental backbone curves for selected WUF-B, WUF-W and RBS connections from the studies mentioned above [6,22,30]. Again, moments have been normalized based on plastic moment capacities reported in the respective studies. Both moments and rotations were computed with respect to the column centerline. In Fig. 3, significant performance improvements derived from almost two decades of research following Northridge are evident. The above overview of special moment connections is not exhaustive as proprietary connections such as the Side Plate™ and Slotted Web™ have met ANSI/AISC performance specifications and have found widespread use in buildings in high seismic areas [29].

As previously stated the performance (ductility), simplicity and economy offered by the RBS when compared to strengthened connections make it especially attractive for new construction. This study proposes an alternative connection strategy through beam weakening which offers comparable ductility to the RBS without the loss of elastic stiffness and buckling resistance as discussed in the following.

2. Introduction to the novel connection concept

The proposed connection utilizes a similar 'fusing' mechanism to that of the RBS, however, weakening of the beam is achieved through a reduction in material strength as opposed to a reduction in flange area. This material strength reduction is achieved through high temperature heat-treatment (annealing) of the beam flanges in the areas highlighted red in Fig. 2b. The temperature history used in the heat-treatment process is shown in Fig. 4a (details provided later) and the resulting softening of the A992 steel is shown in Fig. 4b. As a consequence of this softening, plastic hinging of the beam takes place in the heat-treated beam section (HBS). In a similar manner to the RBS, this connection provides a ductile seismic fuse through weakening, but because the elastic modulus of the HBS is unchanged, a connection modified with such a technique does not sacrifice elastic stiffness as does the RBS. Also, since the cross section of the beam is unaltered and the inelastic portion of the stress strain curve is not significantly modified (note the downward shift of the stress–strain curve in Fig. 4) the buckling resistance of this connection remains similar to that of a beam section before heat-treatment. Another advantage of the HBS connection is that the reduction of plastic hinge moments without the sacrifice of elastic stiffness may lead to more economical columns as panel zone shear demands are lowered. In addition, lower beam flexural strength may lead to reduced column sizes without violating strong column weak beam (SCWB) criteria. The objective of this study was to experimentally validate the HBS concept. Two full scale experiments were conducted and the results are presented below along with details of the heat-treatment method and its development.

3. Heat-treatment thermal process

Annealing heat-treatment of steels is used in the processing and manufacturing of a wide variety of tools, components and equipment. It usually involves heating the steel to a particular temperature followed by a "soak" period and subsequent cooling at a prescribed rate (Fig. 4a). The parameters of the annealing cycle are determined primarily based on the chemical, mechanical and metallographic properties of the alloy prior to annealing and the desired post anneal properties [31]. The body centered cubic to face centered cubic phase transformation that iron undergoes above the lower critical temperature results in the nucleation and growth of new crystal grains upon heating and cooling. Careful control of the heating and subsequent slow cooling typically leads to a courser (larger grain size) grain structure from the annealing process. This coarsening of the grain structure through annealing is primarily responsible for the reduction in strength of A992 steel[2] (Fig. 4b) which is consistent with the well-established Hall–Petch relationship [32]. Optical microscopy images of A992 steel samples before and after annealing are shown in Fig. 5, where coarsening of the grain structure can be seen.

As previously noted weakening of the beam flanges is achieved through a high temperature heat-treatment/annealing process in which the steel is raised to a temperature of 1050 °C and slow cooled to 500 °C after which the steel is left cool in still air to room temperature (Fig. 4a). This process has been designed to reduce the yield and tensile strength of A992 steel by approximately 35% and 25%, respectively. This strength reduction is reflected in the stress strain curves shown in Fig. 4b and summarized along with other material properties in Table 1. Design of this thermal cycle was aided by a parametric study conducted to determine the effect of peak temperature, soak time and cooling rate on the tensile properties of A992. This study was conducted by heat-treating coupons machined from the flange of a W8X39 wide flange member. The heat-treatment was performed in an electric furnace and tested in uniaxial tension in accordance with ASTM A370 [33]. The results are plotted in Fig. 6a and b where it is observed that peak temperature and cooling rate had significant influence on the stress–strain response. It can be seen from both these figures that with higher peak annealing temperatures and slower cooling rates the tensile response is softened (yield strength and tensile strength are lowered). It is also observed that for the ranges of temperatures and cooling rates considered there is no effect on the elastic modulus or the strain at maximum stress (uniform elongation). The effect of the

[2] In this study full annealing is the technique utilized as opposed to *recrystallization* annealing which is typically used to reduce hardness and recover ductility by reducing the defect density in parts which have been heavily cold worked.

Table 1
Summary of material properties of A992 before and after heat-treatment.

Material property	A992	Heat-treated A992
Average grain diameter (μm) (ASTM Size Description)	22.1 (Fine)	56.5 (Medium)
σ_y (ksi)	52.5	32.4
σ_u (ksi)	73.8	54.1
Average Charpy V Notch Toughness @ 70 °F (ft-lb)	72	69
Average HV (Vickers Hardness #)	180	125

Material was obtained from the flange of a W30x148 member.

heat-treatment on fracture strain or material ductility is also insignificant as can be seen in Fig. 6. The sensitivity of strength to peak temperature is explained by the fact that upon austenizing (heating above the upper critical temperature) the growth rate of austenite grains is a thermally activated process so an increase in austenizing temperature (with all other parameters unchanged) results in larger austenite grains.

Austenite grain boundaries tend to be favorable nucleation sites for allotriomorphic ferrite during phase transformation, and so larger austenite (parent phase) grains tend to lead to larger ferrite grains (product phase) [34]. Also grain growth suppressing alloying elements such as niobium, vanadium and aluminum which are often used in A992 steel are less effective at inhibiting growth of austenite grains with increasing temperature. These elements form submicroscopic carbides, nitrides and carbon nitrides which remain undissolved in austenite at high temperatures. These precipitates segregate to grain boundaries during high temperature processing of steels and suppress grain growth through a process known as Zener pining. However, if the temperature is raised above the 'grain-coursing temperature' these precipitates dissolve into austenite and no longer resist grain growth. At this stage there is an abrupt increase in the austenite grain growth rate [32].

Slow cooling during phase transformation facilitates the nucleation and growth of course grained equiaxed ferrite and pearlite with course inter-lamellar spacing from the austenite parent phase. Analogous to dendritic growth during solidification, slower cooling rates during solid state phase transformation tends to yield larger grain sizes due to the available thermodynamic driving force for grain growth (reduction in grain boundary energy) [32]. Careful control of the cooling rate was found to be essential in facilitating purely diffusional phase transformations and promoting the formation of polygonal ferrite and pearlite microstructures. Coupons cooled in still air from high annealing temperatures were observed to form widmanstatten ferrite and banite microstructures which led to higher tensile strength and lower ductility when compared to nonheat-treated coupons.

4. HBS connection design development

Similar to the RBS, three parameters are needed for design of the HBS connection (see Fig. 2), the distance from the column flange to the start of the HBS (dimension a), the length of the HBS (dimension b) and the desired tensile properties of the beam flanges in the HBS. The results of the afore-mentioned parametric study were paired with finite element analysis (FEA) carried out using ANSYS Mechanical ADPL. The FEA was used to evaluate the three main input parameters (dimension a, dimension b and the tensile stress–strain properties of the HBS). The FEA utilized quadratic shell elements (shell 281) and accounted for material nonlinearities through the Chaboche nonlinear kinematic hardening model for the beam and column material and a bilinear kinematic hardening model for the E71T-8 weld material. Geometric non-linearities were accounted for using a large-displacement formulation. The beam flanges and web were assumed to be welded to the column flange in these simulations. The numerical model was first validated against the RBS connection experimental responses from the literature [22]. Subsequently analysis of the HBS connection was performed in order to determine parameters "a", "b" and the desired material strength reduction of the beam flanges in the HBS, for performance evaluation as discussed below. More detail descriptions on the finite element modeling and the constitutive model used are presented in Ref. [35].

The FEA study revealed that dimensions similar to those specified in 2010 ANSI/AISC 358 for RBS parameters "a" and "b" provides desirable performance for the HBS connection. Distance "a" was kept as small as possible to maximize moment reductions at the face of the column without causing high strain demands at the beam flange complete joint penetration (CJP) welds. While dimension "b" was proportioned so as to provide a large region over which yielding of the beam flange is promoted. This allows a wide distribution of plasticity which helps to provide high energy dissipation, stable hysteretic behavior and lowers strain demands in the HBS region. When combined with the same dimensions for "a" and "b", the tensile properties of heat-treated A992 steel shown in Fig. 4b were found to provide similar strength (moment capacity) reduction to RBS flange area reductions of 40%.

Results of these FEA analysis are shown in Fig. 7 in which comparisons are made between the global and local responses of RBS and HBS connections having the same beam and column sizes and the same dimensions for parameters "a" and "b" along with similar reductions in moment capacity in the weakened section. Fig. 7b shows the moment-rotation envelop (in positive bending) comparison in which it is observed that the HBS connection provides improved elastic stiffness (~7% increase) and delayed onset of strength degredation as compared to the RBS. In this figure moments have been nomrmalized

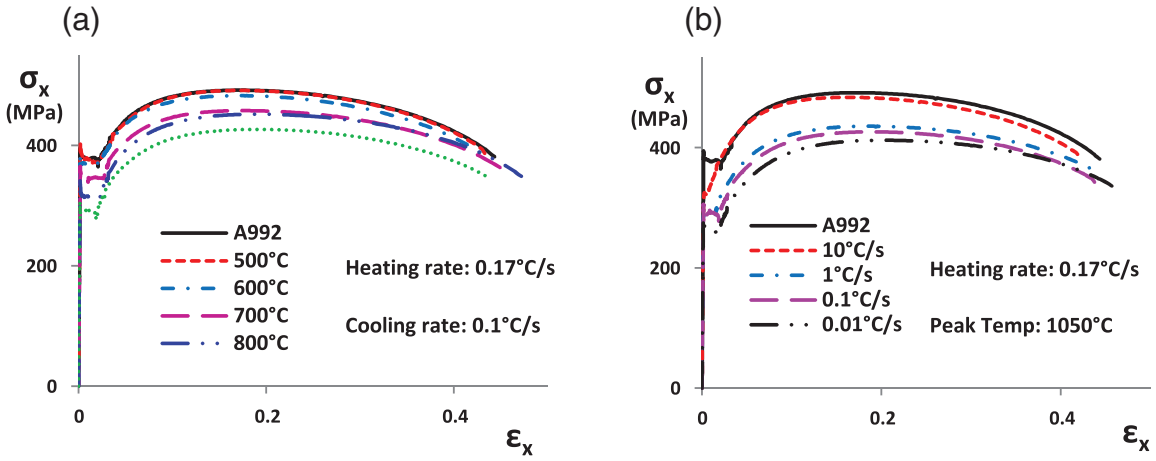

Fig. 6. Uniaxial stress strain responses of heat-treated A992 Steel: (a) effect of peak temperature and (b) effect of cooling rate.

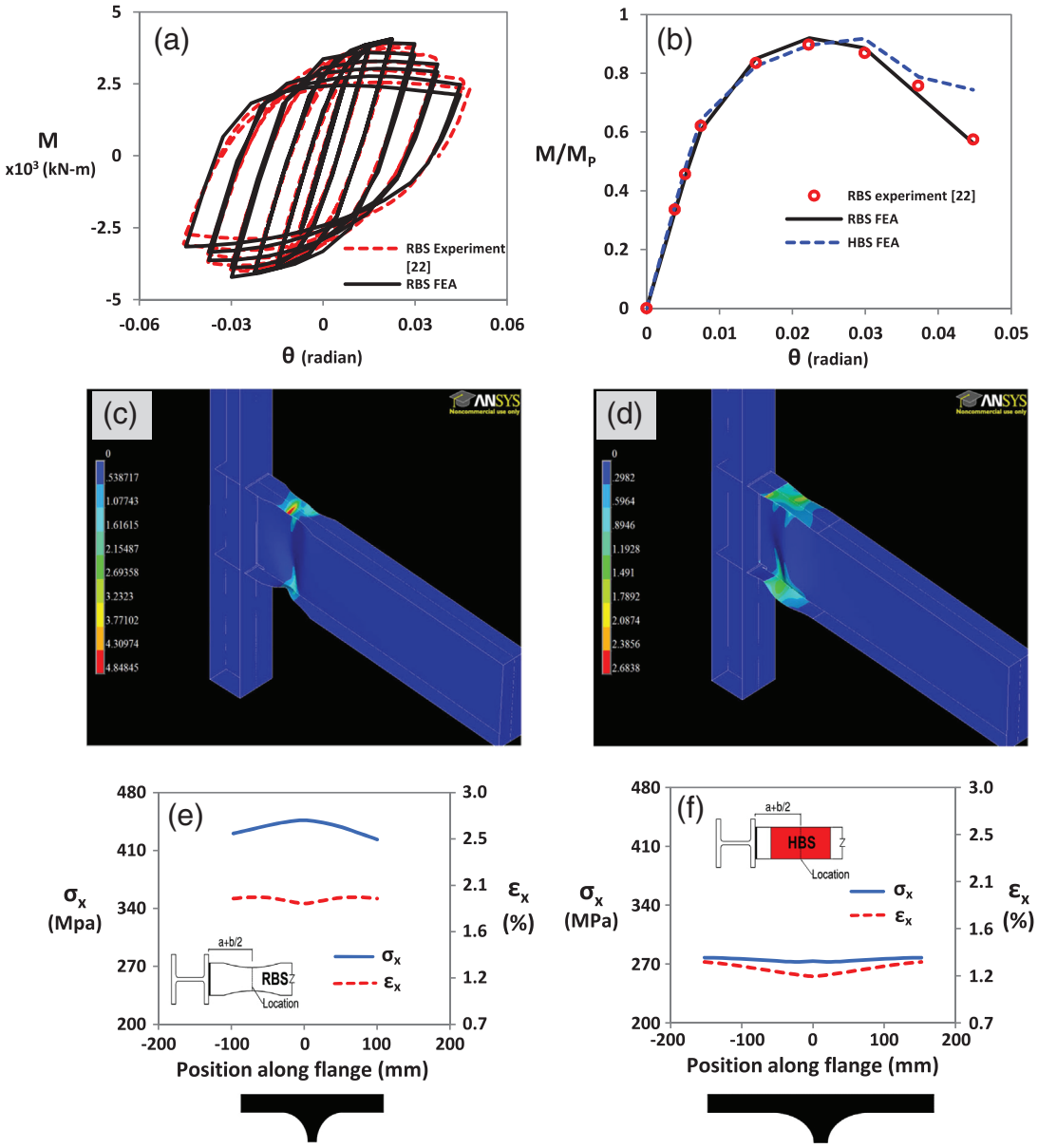

Fig. 7. Finite element analysis of RBS and HBS connections: (a) comparison of experimental and analytical results for specimen DB 3 Engelhardt et al. [22]; (b) comparison of M-θ envelop (Moments are normalized to the plastic moment capacity of the beam at the face of the column); (c) equivalent plastic strain solution of RBS @ 4.5% story drift; (d) equivalent plastic strain solution of HBS @ 4.5% story drift; (e) longitudial stress and strain at the center of the RBS @ 2% story drift; (f) longitudial stress and strain at the center of the HBS @ 2% story drift.

to the plastic moment capacity of the unweakened crossection adjacent to the column face and rotations are computed at the face of the column. Note also that the HBS connection provides relocation of the plastic hinge similar to that of the RBS connection as indicated in Fig. 7c and d which shows a contour plot of the equivalent plastic strain responses for both connections.

From comparison of Fig. 7e and f it is observed that though both the RBS and HBS create a fuse through weakening, in a strict sense, there is a difference in the local stress and strain state within the weakened region in both connections. For example at 2% drift the longitudinal stresses and strains in the RBS are higher than those in the HBS as can be observed by comparing these figures. This can be explained by considering that in the case of the RBS yielding is promoted in the reduced flange section due to higher effective stresses in this area (relative to the unreduced section adjacent to the column) resulting from the area reduction. However, in the HBS, stresses in the weakened region are lowered due to the reduction in material strength. This stress reduction provides added benefit in terms of local buckling resistance, especially if this technique is applied to flanges and webs of sections with slender elements. Further, it is noted that the HBS provides a constant reduction of material strength over the entire weakened region while the strength reduction in the RBS is concentrated in the center of trimmed flange. As a result of this, inelastic action in the form of yielding is distributed over a larger flange area in the HBS as compared to the RBS (Fig. 7c and d); this reduces strain demands despite providing a similar 'fuse' mechanism through weakening.

5. Heat-treatment method for full scale beams

In the current study heat-treatment of the beam flanges was performed after fabrication of the beam was complete but prior to field welding the beam to column. Heat-treatment was accomplished via the use of electric surface heating pads which were attached to both the outside and inside surfaces of the beam flanges as shown in Fig. 8a and c. These heating pads are constructed from a nickel-iron alloy electric resistance heating wire woven through ceramic beads

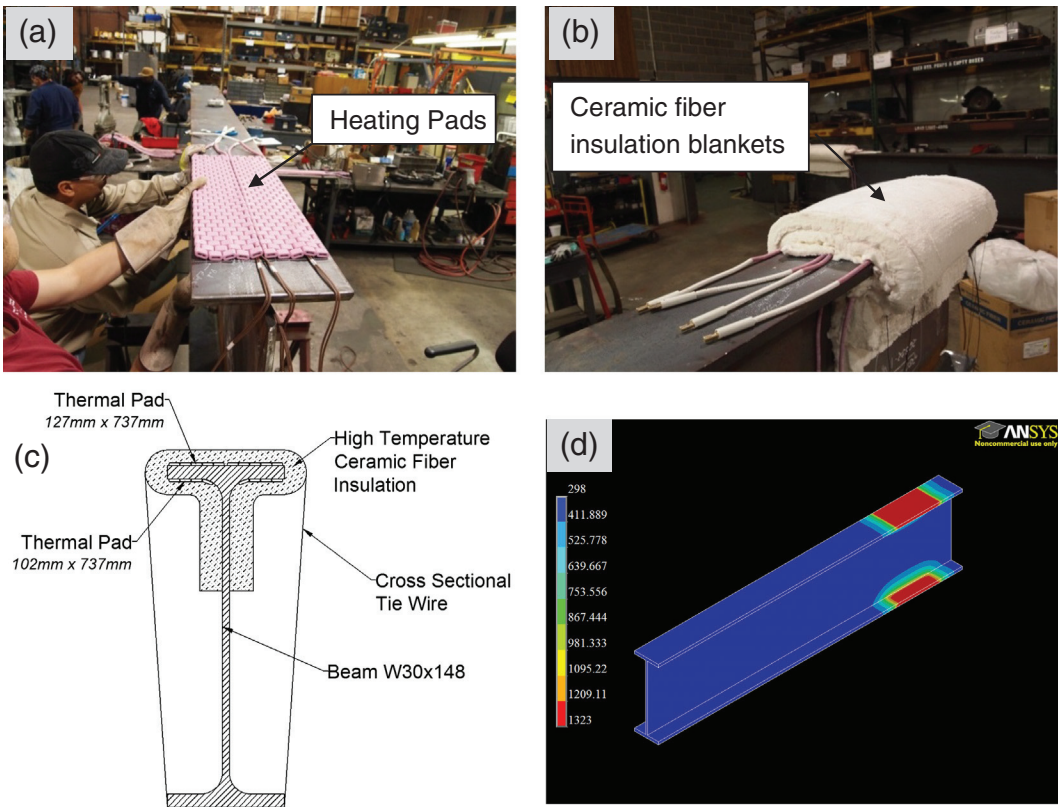

Fig. 8. Heat-treatment setup: (a) photograph showing electric surface heating pads during installation on a beam flange, (b) photograph showing insulation of beam flange for well controlled heating and cooling, (c) schematic showing section view of heat-treatment setup, and (d) contour plot from thermal finite element analysis [36] of temperature (absolute scale) distribution during heating of the beam.

which were sized based on the dimensions of the heat-treated region. Power is supplied to the heating pads via a portable power console and type K thermocouples were used to measure temperatures and provide continuous feedback to the power console controller. The heat-treatment set-up was completed by enclosing the beam flange and part of the beam web with two layers of 2″ high density ceramic fiber insulation blankets as shown in Fig. 8b.

No heat sinks were needed to prevent heat conduction to regions of the beam outside of the HBS. FEA was used to perform thermal simulations to analyze temperature distribution during heating and cooling [36]. These analyses predict that regions outside the HBS remain at temperatures below 500 °C during the heat-treatment process (see Fig. 8d) and as a result, no significant change in strength is expected in these areas. This can be deduced from the results of tensile tests conducted on coupons subjected to peak temperatures of 500 °C and 600 °C shown in Fig. 6a. This was also confirmed via tensile testing of coupons taken from the beam flange adjacent to the HBS during the development of the full scale heat-treatment process. Thermal analysis predictions were later confirmed by temperature measurements made using type K thermocouples and infrared thermometers during the heat-treatment of beam specimens. No distortion of the beam sections were observed after the completion of the full scale heat-treatment process.

6. Connection design and experimental setup

Two identical large scale specimens (HBS 5 and HBS 7) were tested to validate the HBS concept. See Fig. 9a and c for the test setup. In these specimens the HBS was combined with an all welded connection in which the beam flanges and web were connected to the column flange using complete joint penetration welds. These details are consistent with current design and construction practice for RBS connections utilized in SMFs. The beam and column sections and lengths were chosen to be similar to those of specimen DB5 studied by Engelhardt et al. [22]. However, the column panel zone was reinforced with two-12.7 mm (1/2 inch) doubler plates which were designed to promote strong panel zone behavior and ensure that most of the inelastic action was obtained from the beam. By doing this, large plastic rotation demands are placed on the beam which allows better evaluation of the ductility and energy dissipation provided by the HBS. These connection details are shown in Fig. 9b.

Connection welding was performed outdoors with the column oriented vertically by a welder qualified in accordance with the requirements of AWS D1.1-10 and AWS D1.8-09. Welding was accomplished with self-shielded flux cored arc welding (FCAW) process. E70-T6 electrodes were used for beam flange welds, while E71-T8 electrodes were used for the beam web weld and the reinforcing fillet welds. Both of these electrodes were specified by the manufacturer to deposit metal with a minimum Charpy V-notch toughness of 27 J (20 ft.-lbs.) at −28 °C (−20 °F). The bottom flange backing bar was removed and a reinforcing weld was placed at the root of the grove weld.

The top flange backing bar was left in place, however a fillet weld was provided between the backing bar and the column flange. Weld tabs from the top and bottom beam flange groove welds were removed by carbon air arc gouging. No vertical weld tabs were used for the beam web CJP welds. Finally, all CJP welds were ultrasonically (UT) tested by a certified welding inspector (CWI) in conformance with AWS D1.1-10 and AWS D1.8-09.

7. Instrumentation

Each specimen was equipped with strain gauges along the beam flanges to monitor longitudinal flange strains, at various locations including the weld toe and HBS region. String and linear potentiometers were used to monitor displacements and rotations in the column,

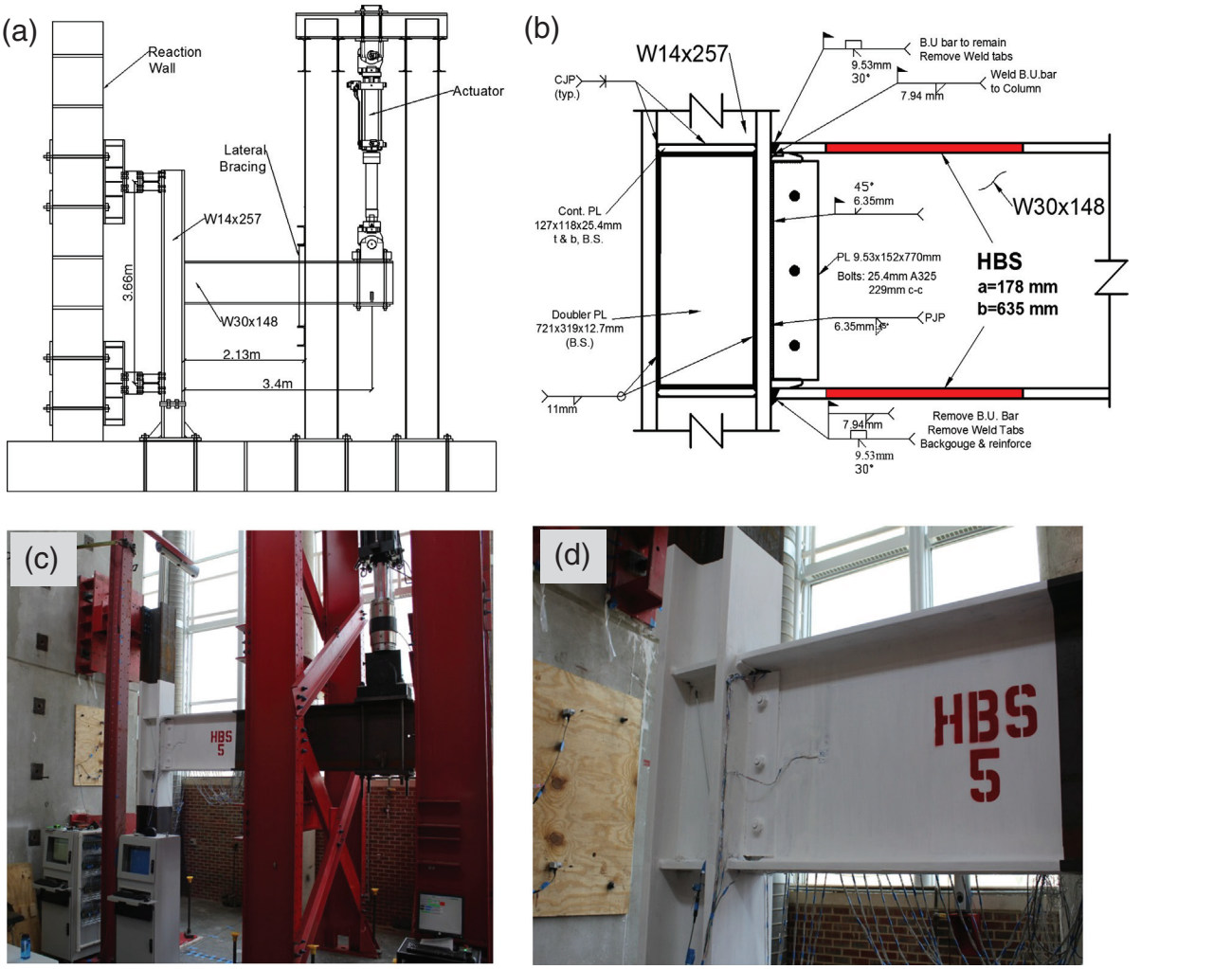

Fig. 9. HBS test setup and connection details: (a) sketch of the test setup, (b) sketch of the connection details, (c) photograph showing test setup, and (d) photograph of HBS 5 connection prior to testing.

beam and panel zone. A calibrated load cell in the hydraulic actuator provided readings of force response during the experiment. All specimens were painted with hydrated lime prior to testing to visually indicate regions of yielding.

The Optotrak Certus HD three-dimensional (3D) position system produced by Northern Digital Incorporated was used to capture the positions of markers placed along the beam flanges and web as shown in Fig. 10. Two Optotrak cameras were used which were able to capture the motion of markers placed on the top and sides of the beam top flange, the beam web and the side of the beam bottom flange. Position time history data obtained from this system was post processed to calculate displacements and strains in areas of interest. Accuracy of the Optotrak system was illustrated by Goodnight et al. [37] where the strain measurements obtained from the Optotrak system were found to closely match those measured by traditional instruments (strain gage and extensometer) for a tensile test of a steel bar. The

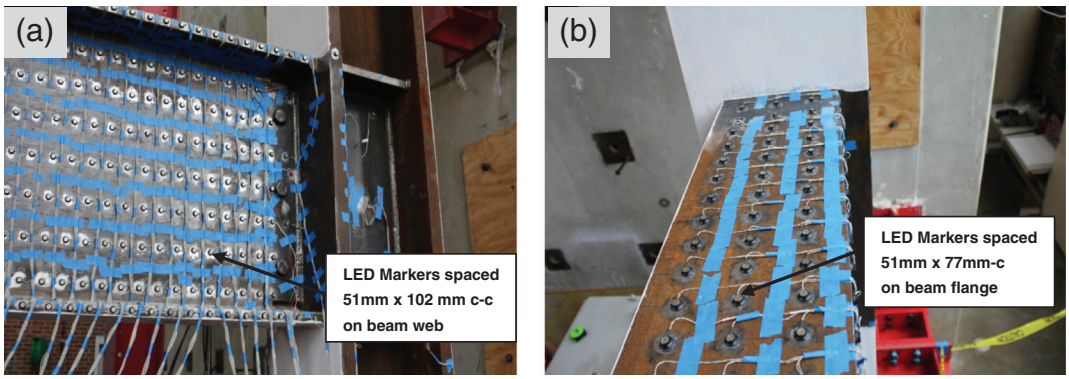

Fig. 10. Instrumentation of HBS 5: (a) LED markers placed on beam web and the sides of beam top and bottom flanges, and (b) LED markers placed on beam top flange.

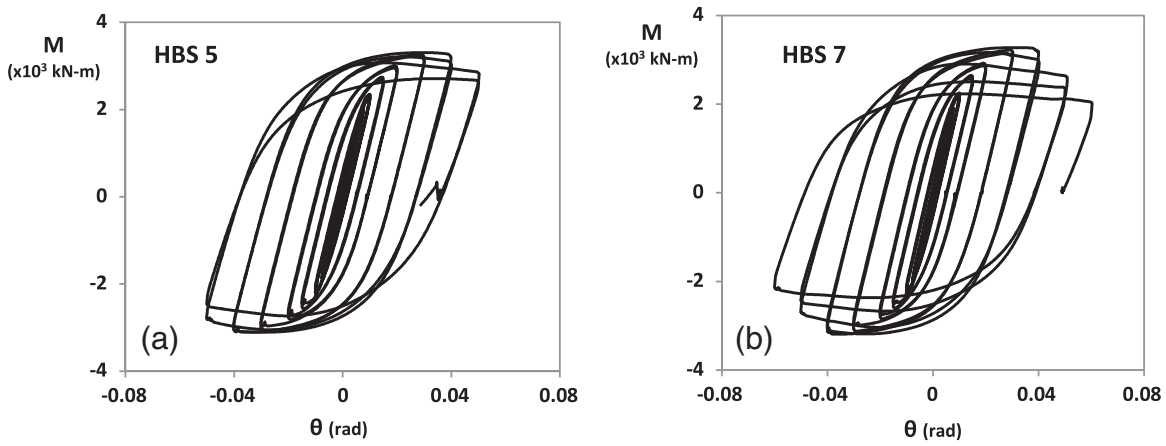

Fig. 11. Moment-rotation responses of HBS connections: (a) HBS 5 and (b) HBS 7.

Optotrak system provides the advantage of being able to record large cyclic inelastic strains while electrical resistance strain gages may either exhibit gradual strain drift or fail to remain adhered.

8. Test results

8.1. Global response of HBS connections

Testing was conducted at the North Carolina State University Constructed Facilities Laboratory (CFL) on an exterior type sub-assemblage (single cantilever). Loads were applied at the beam tip in accordance with the 2010 ANSI/AISC 341 [18] seismic provisions Appendix S loading protocol consisting of quasi-static increasing amplitude displacement cycles. Fig. 11 shows the moment-rotation response of both specimens. These global responses of HBS connections show wide hysteresis loops indicating good energy dissipation. Both specimens exceeded the 2010 AISC Seismic Provisions (ANSI/AISC 341-10) SMF qualifying 4% interstory drift angle without significant strength loss. Strength degradation due to local flange, web and lateral torsional buckling initiated during the 2nd cycle of loading at 4% drift (see Fig. 11a) and continued

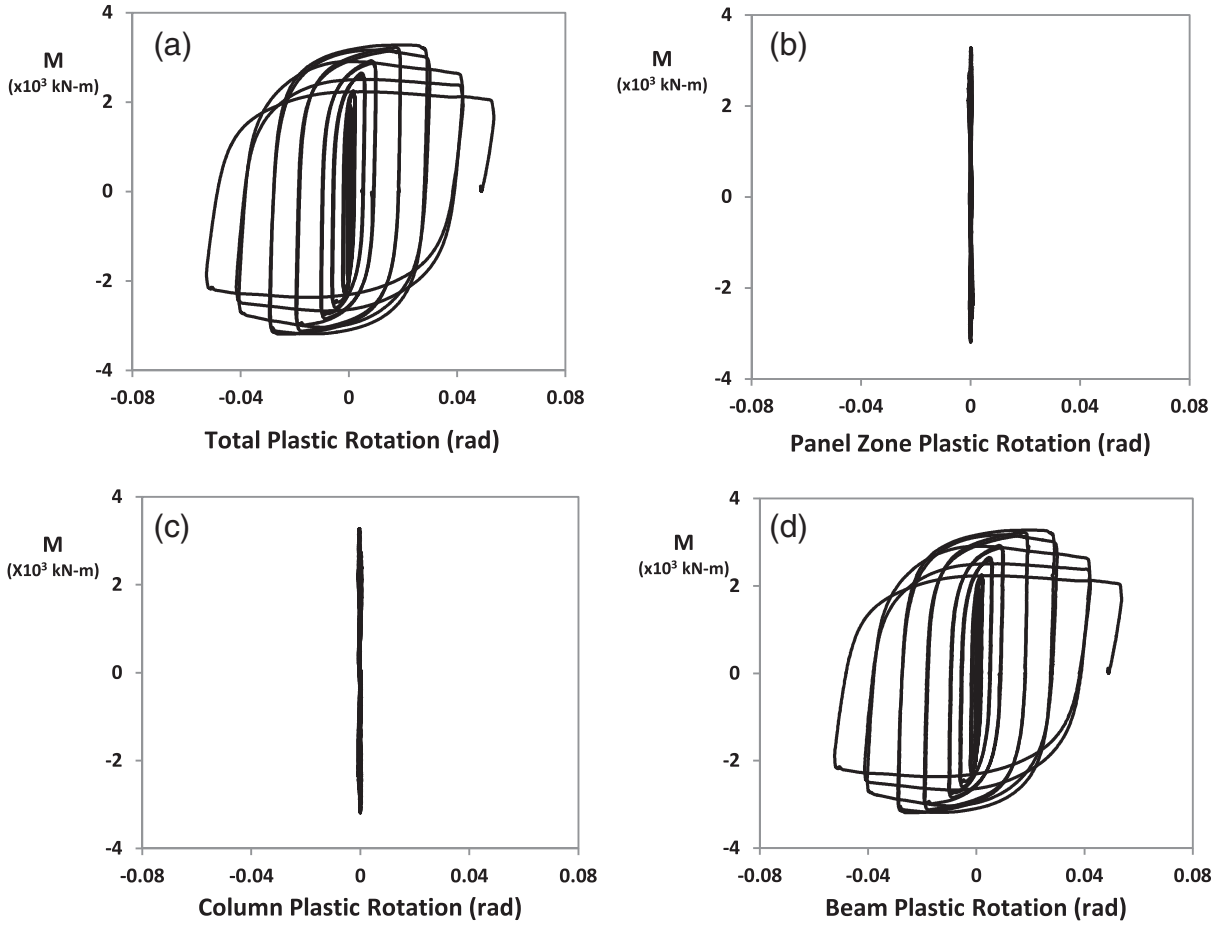

Fig. 12. Plastic rotation contributions by components of HBS 7: (a) total connection plastic rotation, (b) panel zone shear plastic rotation, (c) column flexural plastic rotation and, (d) beam plastic rotation.

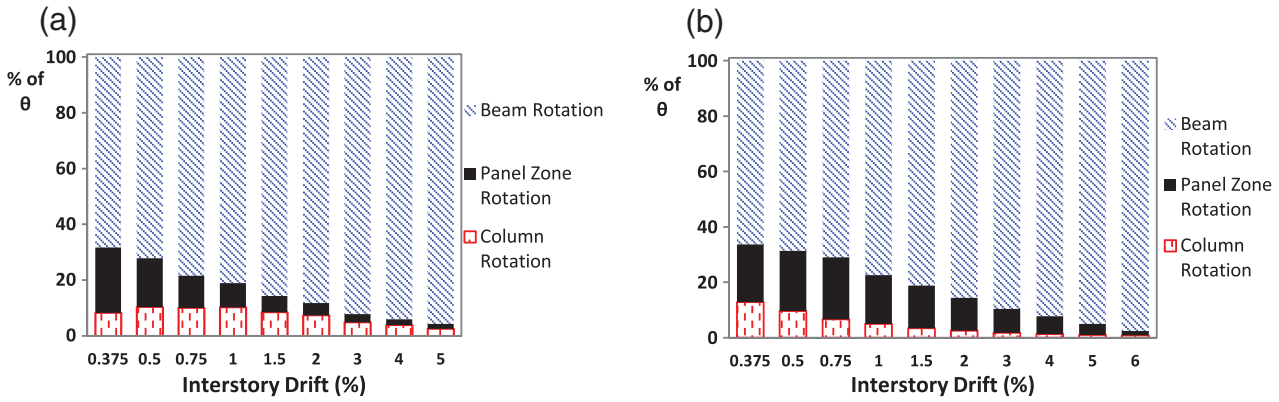

Fig. 13. Total rotation contributions of HBS connections: (a) HBS 5 and (b) HBS 7.

during later loading cycles. Loading of HBS 5 was terminated after sustaining two loading cycles at 5% drift due to a fracture in the location of significant flange buckling. Loading of HBS 7 was terminated before starting the 2nd loading cycle at 6% story drift (see Fig. 11b) due to significant strength loss as a result of lateral buckling and twisting of the beam.

The response of the HBS 7 is further analyzed by plotting the moment-plastic rotation curves for each component of the connection assembly which were calculated using data measured by instrumentation during the test and equations proposed by Popov et al. [38]. These graphs as shown in Fig. 12 indicate that panel zone shear and column flexural deformations contributed only to the elastic behavior of the sub-assemblage and as a result, inelastic action was entirely confined to the beam. The contributions of panel zone shear and column flexural deformations to the total rotation of the connection are observed to diminish as loading amplitudes are increased.

This is illustrated in Fig. 13 which presents bar graphs of the total rotation contributions (elastic + plastic) of each component to the total connection rotation for both specimens. The trends observed in both graphs confirm the expectation for beam hinge rotations to dominate the deformations by a continuously greater magnitude as imposed drift angles are increased in ductile connections with strong panel zones designed to satisfy strong column weak beam criteria.

8.2. Plastic hinge formation in HBS connection

Fig. 14 illustrates the progression of inelastic action along the beam flange via bar graphs in which the distribution of longitudinal tensile strains (normalized by the yield strain) along the centerline of the beam flange at various stages of the loading history are plotted. Bars highlighted in red represent the strains in the heat-treated (weakened) regions. Strains were calculated by post processing data obtained from

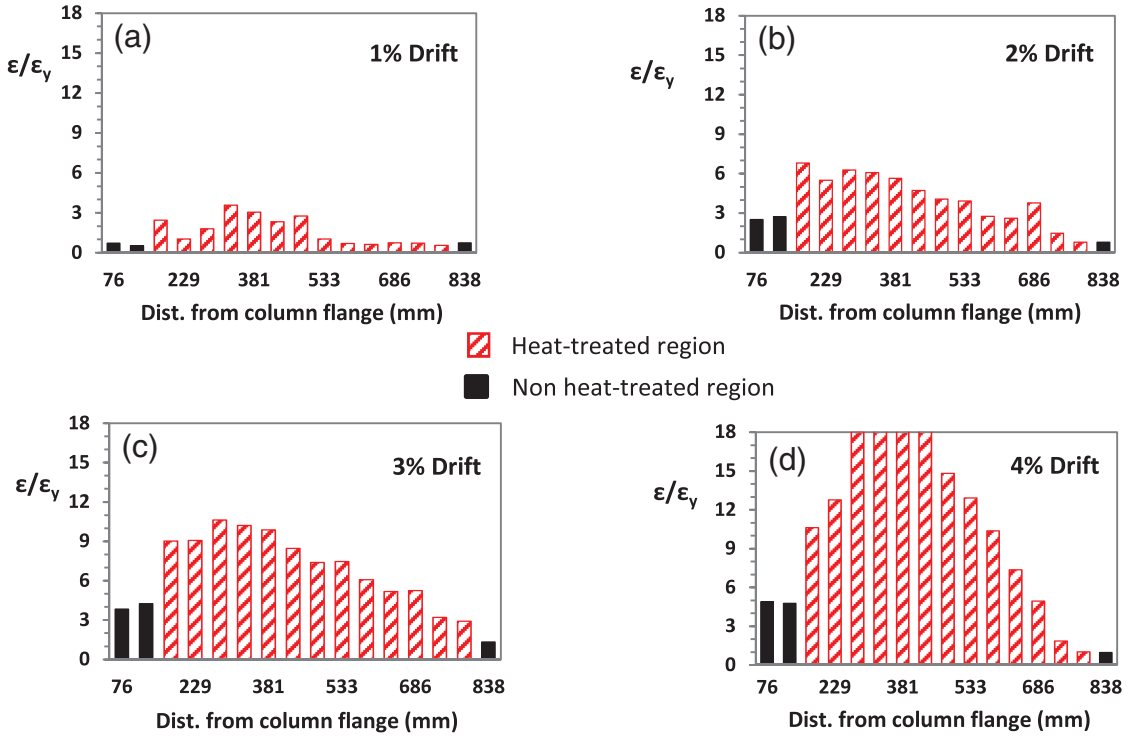

Fig. 14. Recorded longitudinal strains along the center of top flange of the beam from HBS 5.

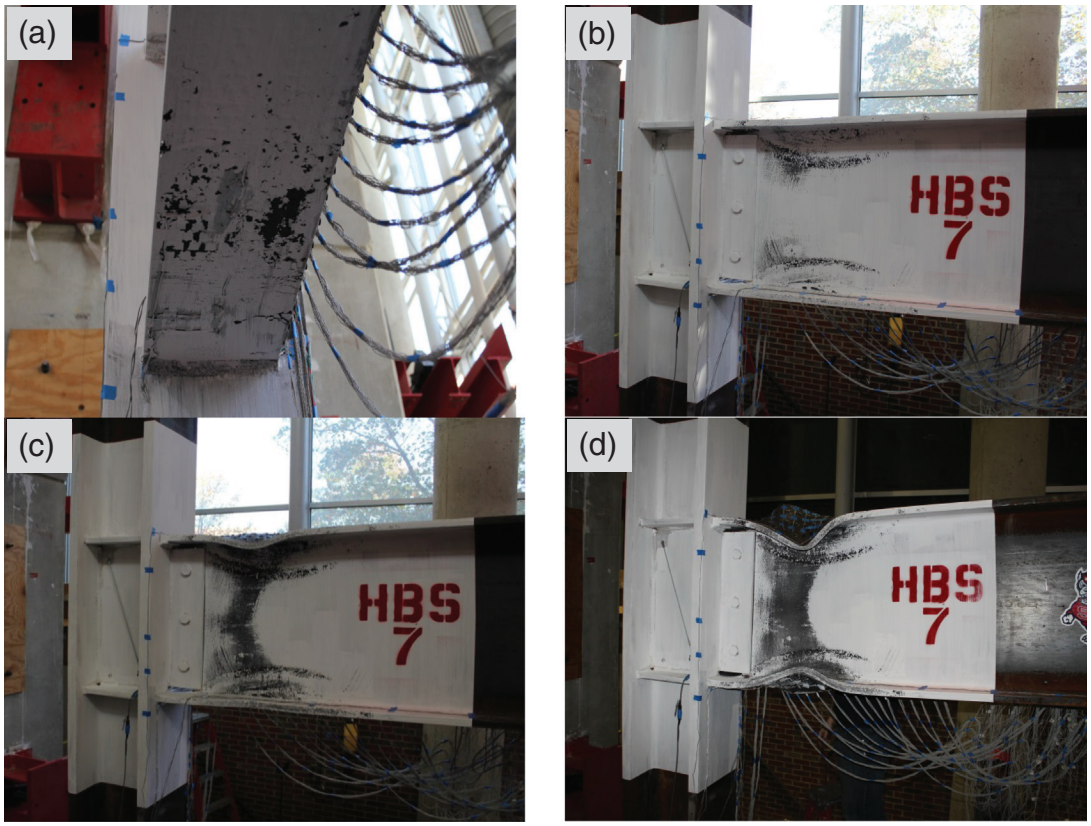

Fig. 15. Yielding and plastic hinge formation of HBS 7: (a) view of beam bottom flange at 1% drift, (b) connection at 3% drift, (c) connection at 4% drift and (d) connection at 6% drift.

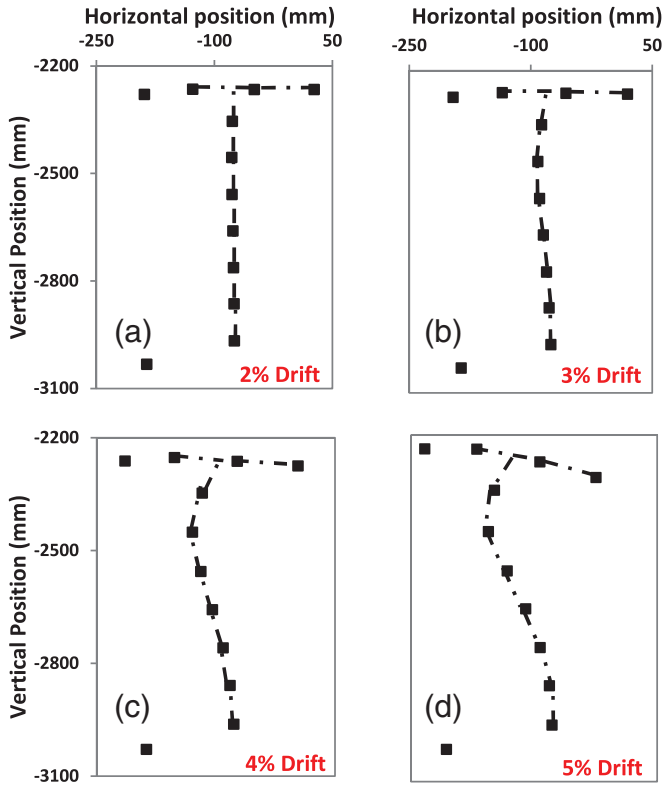

Fig. 16. HBS 5 progression of beam web and flange buckling recorded 406 mm away from the column flange at interstory difts of (a) 2%, (b) 3%, (c) 4% and (d) 5% (beam is in positive bending i.e. top flange in compression).

3D noncontact spatial displacement measurement sensors placed along the beam flange as shown in Fig. 10. These plots demonstrate proof of the HBS concept and the following observations have been made:

1. Flexural yielding of the beam flange initiated within the HBS as evidenced by strains recorded at 1% interstory drift (Fig. 14a) and flaking of white wash observed during testing (Fig. 15a).
2. As loading amplitudes were increased, strains within the HBS and near the column face increased and the distribution of strain within the heat-treated areas were influenced by the moment gradient. It is of note that the beam tested had a length of 3.4 m (134 inches) corresponding to a moment frame with a clear span of approximately 6.8 m (22 feet). This relatively short span results in a large moment gradient which when combined with the strain hardening of the heat-treated material results in some limited yielding near the column face. However this was not observed to have a detrimental effect on the performance of the HBS connections as no weld or near weld failures were observed.
3. As the loading progresses from 2% to 4% drift, strains within the HBS increase significantly while strains adjacent to the column face grow slightly (see Fig. 14b–d). Also at 4% drift large strains are distributed over a significant length of the HBS region. These indicate that large displacements imposed at the beam tip are mostly accommodated by inelastic flexural action in the HBS through gradual formation of the plastic hinge.

8.3. Failure mechanism of HBS connections

As previously stated, strength degradation of both specimens began during the 2nd cycle of loading at 4% drift when significant local beam web, flange and lateral torsional buckling was observed (see Figs. 11 and 15c). To demonstrate the progressive strength degradation mechanism, beam cross-sections located at 406 mm away from the column

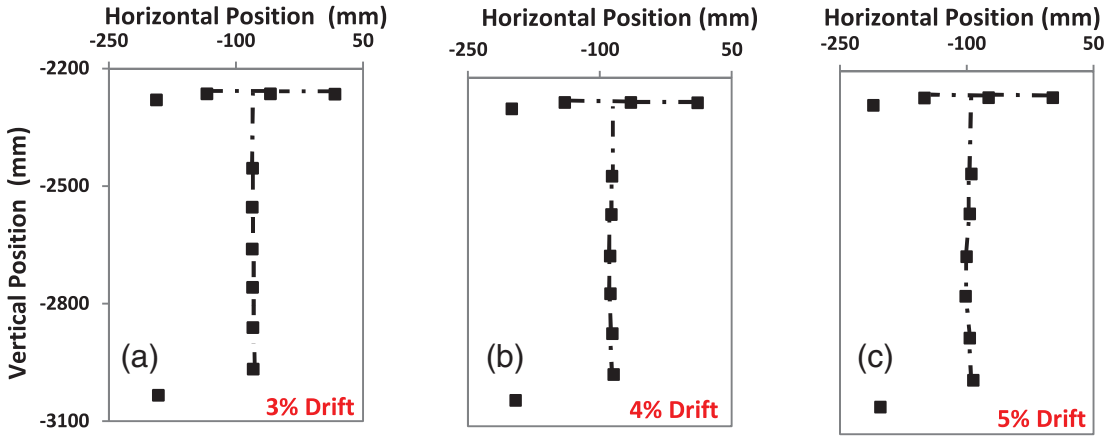

Fig. 17. HBS 5 progression of beam web and flange buckling recorded 106 mm away from the column flange of HBS 5 at interstory drifts of (a) 3%, (b) 4% and, (c) 5% (beam is in positive bending i.e. top flange in compression).

flange (within the HBS) are plotted using the recorded vertical and horizontal positions of Optotrak markers of HBS 5 at various peak drift rotations as shown in Fig. 16. Dotted lines have been traced between data points to make evident the progressive buckling of the beam.

In this figure it is observed that the degradation mechanism appears to have been initiated by slight local buckling of the beam web in the plastic hinge during loading cycles at 3% interstory drift (Fig. 16b). This local web buckling was soon followed by local flange buckling and twisting of the beam as the loading amplitude was increased (Fig. 16c). The amplitudes of flange and web buckling gradually increased with the rotation amplitude resulting in the observed strength degradation (Figs. 11 and 16). This progressive strength degradation mechanism was observed in both test specimens. Testing of HBS 7 was stopped as a result of this significant strength loss. In the case of HBS 5, rupture of the beam flange at the region of largest buckling amplitude is believed to be a result of large strain due to localized bending of the beam flange resulting from the afore described degradation mechanism rather than an axial stress effect. This was also observed in extended end plate (EEP) and welded unreinforced flange-bolted web (WUF-B) connections modified with the HBS technique [39,40].

Fig. 17 shows a series of similar beam cross-section plots of markers located 106 mm away from the column flange (between the column flange and the HBS). Comparison of beam cross-sections in Fig. 17 to those in Fig. 16 with the same drift reveals that in addition to reducing strain demands near the column face as previously discussed (Fig. 14), the HBS was also successful in shifting large deformations due to beam web and flange buckling away from the beam flange CJP welds. Inspection of Figs. 16d and 17c shows that at 5% drift only very slight lateral deformations are evident close to the column flange while significant lateral displacement and twisting of the beam are observed in the plastic hinge. Post-test measurements (Fig. 18) showed flange buckling amplitudes between 114 mm (4.5 inches) and 152 mm (6 inches) and web buckling amplitudes between 80 mm (3 inches) and 127 mm(5 inches) in the two specimens. These large buckling amplitudes were located approximately 420 mm (16.5 inches) from the column flange.

Fig. 18. Photograph showing post-test local flange buckling amplitude of HBS 7 (after one cycle of 6% drift).

8.4. Comments on a possible design method of HBS connections

The limited number of tests conducted in this program is insufficient to develop a design method for HBS connections. However, analysis of the available experimental data shows that a design methodology similar to that currently used for RBS connections may be adopted. Table 2 presents data on the magnitudes of bending moments developed in both specimen beams. These were compared to the estimated plastic moment capacity of the un-weakened beam section adjacent to the column flange calculated from measured tensile coupon data. Bending moments developed in the middle of the HBS were compared to the estimated plastic moment capacity based on estimated tensile properties obtained from prior tensile testing of coupons extracted from undamaged heat-treated beam flanges.

Maximum bending moments at the face of the column were 5–8% higher than the plastic moment capacity while bending moments at the center of the HBS were 26–29% higher that the plastic moment capacity of the weakened section indicating significant work hardening. These results are comparable with RBS test data presented in Engelhardt et al. [22].Therefore a design methodology in which the parameters of the HBS are selected so as to limit the bending moments at the column face to a desired factor of the plastic moment capacity can be developed. Note that the proposed heat-treatment may also be applied to the beam web in addition to the flanges if design scenarios require larger reduction of moments at the column flange.

9. Conclusion

The experimental validation of an innovative seismic performance enhancing technique for welded steel moment connections has been presented. The technique involves weakening regions of the beam flanges away from the welded joint by exposing them to high temperatures followed by slow cooling. Consequently, under simulated seismic loading, plastic hinging of the beam takes place in the heat-treated beam section (HBS). All welded connections enhanced with the HBS displayed ductile seismic response, which exceeded the 2010 AISC Seismic Provisions (ANSI/AISC 341-10) SMF qualifying 4% interstory drift angle without

Table 2
Bending moments developed in HBS test specimens.

Specimen Beam	F_y* (Mpa)	M_p (kN-m)	$M_{p\text{-HBS}}$ (kN-m)	M_{max} (kN-m)	$M_{max\text{-HBS}}$ (kN-m)	M_{max}/M_p	$M_{max\text{-HBS}}/M_{p\text{-HBS}}$
HBS 5 W30x148	362	2966	2109	3118	2664	1.26	1.05
HBS 7 W30x148	344	2819	2005	3037	2595	1.29	1.08

M_p = plastic moment of beam based on flange tensile coupon data.
$M_{p\text{-HBS}}$ = plastic moment at center of HBS region based on estimated flange yield stress.
M_{max} = maximum moment developed at column face.
$M_{max\text{-HBS}}$ = maximum moment developed at center of HBS region.
* Flange yield strength determined from tensile coupons tested in accordance with ASTM A370.

much strength loss. Test data also shows that the HBS was successful in shifting the majority of inelastic action and lateral deformation due to local flange and web buckling away from the welded joint.

Based on the results of this preliminary study the HBS concept shows promise as a means of providing a simple, ductile, seismic fuse without sacrificing elastic stiffness or buckling resistance. As a result, other applications of this concept may appear fruitful where these characteristics are desired. For example, this concept has also been successfully used to enhance the seismic performance of extended end plate (EEP) and welded unreinforced flange bolted web (WUF-B) moment connections [39,40]. This technique may also prove useful in enhancing the seismic performance of link to column connections in eccentrically braced frames or providing low yield strength steel for use in steel plate shear walls. Given the wide scope of possible applications of this technique, future studies are needed to implement it to end uses where it may provide the optimal combination of performance and economy.

Despite, the promising results presented in this study, more analytical and experimental investigation is needed for further development and eventual industry implementation of HBS moment connections. Experimental studies are needed to evaluate the suitability of this technique for a range of beam and column sections, especially larger and heavier sections which experience more severe strain concentrations during seismic loading [41]. Numerical and analytical parametric studies may be paired with such experimental investigations to develop reliable design methods for accurately predicting strength and performance limit states of HBS moment connections.

Acknowledgment

Funding for this research was provided by the National Science Foundation under the Network for Earthquake Engineering Simulation (NSF Grant no. 0936547). However, any opinions presented in this paper are solely those of the authors. The authors greatly acknowledge the efforts and assistance provided by the staff of Furmanite Inc., Steel Fab Inc., Flores Welding Inc. and the Constructed Facilities Laboratory (CFL) at NCSU. The assistance of Prof. Micheal Engelhardt of the University of Texas at Austin with developing welding procedures is much appreciated. Also, in-kind support provided by Skanska USA building and CMC South Carolina Steel is gratefully acknowledged.

References

[1] Kunnath SK, Malley JO. Structural forum. J Struct Eng 2000;126(1):4–9.
[2] Youssef NFG, Bonowitz D, Gross JL. A survey of steel moment-resisting frame buildings affected by the 1994 Northridge earthquake. Report NISTIR 5625. Maryland: National Institute of Standards and Technology NIST Gaithersburg; 1995.
[3] Popov EP, Yang T, Chang S. Design of steel MRF connections before and after 1994 Northridge earthquake. Eng Struct 1998;20(12):1030–8.
[4] Stojadinovic B, Subhash CG, Lee K-H, Margarian AG, Choi J-H. Parametric tests on unreinforced steel moment connections. J Struct Eng 2000;126:40–9.
[5] Han SW, Kwon GU, Moon KH. Cyclic behavior of post-Northridge WUF-B connections. J Constr Steel Res 2007;63:365–74.
[6] Ricles JM, Mao C, Lu LW, Fisher JW. Inelastic cyclic testing of welded unreinforced moment connections. J Struct Eng 2002;128(4):40–9.
[7] Bruneau M, Uang CM, Whittaker A. Ductile design of steel structures. New York: McGraw Hill Companies; 1998.
[8] Krawinkler H, Popov EP. Seismic behavior of moment connections and joints. J Struct Div 1982;108:373–90.
[9] Engelhardt M, Husain AS. Cyclic-loading performance of welded flange-bolted web connections. J Struct Eng 1993;119(12):3537–50.
[10] Barsom JM, Pellegrino JV. Failure analysis of welded steel moment-resisting connections. J Mater Civ Eng 2002;14(1):44–9.
[11] Xue M, Kaufmann EJ, Lu L, Fisher JW. Achieving ductile behavior of moment connections-Part II. Mod Steel Constr 1996;36(6):38–42.
[12] Sumner EA, Murray TM. Behavior of extended end-plate moment connections subject to cyclic loading. J Struct Eng 2002;128(4):501–8.
[13] Engelhardt MD, Sabol TA. Testing of welded steel moment connection in response to the Northridge earthquake. Progress report to AISC committee on special moment-resisting frame research, October; 1994.
[14] Adan SM, Gibb W. Experimental evaluation of Kaiser Bolted Bracket steel moment-resisting connections. Eng J 2009:181–95.
[15] Uang CM, Yu QS, Noel S, Gross J. Cyclic testing of steel moment connections rehabilitated with RBS or welded haunch. J Struct Eng 2000;126(1):57–68.
[16] Schneider SP, Teeraprbwong I. Inelastic behavior of bolted flange plate connections. J Struct Eng 2002;128:492–500.
[17] Sato A, Newell J, Uang CM. Cyclic testing of bolted flange plate steel moment connection for special moment frames. Report No. SSRP-07/10 Department of Structural Engineering. San Diego, Lo Jolla, CA: University of California; 2007.
[18] AISC/ANSI 341-10. Seismic Provisions for structural steel buildings, Chicago; 2010.
[19] AISC/ANSI 358-10. Prequalified Connections for special and intermediate steel moment frames for Seismic Applications, Chicago; 2010.
[20] SAC Joint Venture. Behavior and design of radius cut reduced beam section connections. Rep. No. SAC/BD-00/17; 2000.
[21] Plumier A. The dogbone: back to the future. Eng J 1997;34(2) [2nd Quarter].
[22] Engelhardt M, Winneberger T, Zekany A, Potyraj T. Experimental investigation of dogbone moment connections. Eng J 1998;35(4):128–39.
[23] Chi B, Uang CM. Cyclic response and design recommendations of reduced beam section moment connections with deep columns. J Struct Eng 2002;128:464–73.
[24] Kim K-D, Engelhardt MD. Nonprismatic beam element for beams with RBS connections in steel moment frames. J Struct Eng 2007;133(2):176–84.
[25] Jones SL, Fry GT, Engelhardt MD. Experimental evaluation of cyclically loaded reduced beam section moment connections. J Struct Eng 2002;128:441–51.
[26] SAC Joint Venture. Cyclic response of RBS moment connections: loading sequence and lateral bracing effects. Rep. No. SAC/BD-00/22; 2000.
[27] Lee D, Cotton SC, Hajjar JF, Dexter RJ. Cyclic behavior of steel moment-resisting connections reinforced by alternative column stiffener details, I. Connection performance and continuity plate detailing. Eng J 2005:189–213 [4th Quarter].
[28] SAC Joint Venture. Parametric tests on the free flange connections. Rep. No. SAC/BD-00/02; 2000.
[29] FEMA-350. Recommended seismic design criteria for new steel moment-framebuildings. prepared by the SAC Joint Venture for the Federal Emergency Management Agency, Washington, DC; 2000.
[30] SAC Joint Venture. Parametric tests on unreinforced connections Volume 1- Final report. Rep. No. SAC/BD-00/01; 2000.
[31] Bramfitt BL. Annealing of steel. Heat treatingASM Handbook, vol. 4. ASM International; 1991 42–55.
[32] Krauss G. Steels: processing, structure, and performance. ASM International; 2005.
[33] ASTM A370-10 Standard Test Methods and Definitions for Mechanical Testing of Steel Products; 2010.
[34] Siwecki T, Engberg G. Recrystallization controlled rolling of steels. Proceedings: thermomechanical processing in theory, modelling, and practice; 1996.
[35] Morrison M, Hassan T. Significance of constitutive models in the seismic simulation of welded steel moment connection responses. J Struct Eng 2015 [submitted for publication].
[36] Quayuum, S. & Hassan, T. "Thermal analysis of heat-treated beams for HBS connection," (Unpublished results), NC State University, 2011.
[37] Goodnight JC, Kowalsky MJ, Nau JM. Effect of load history on performance limit states of circular bridge columns. J Bridg Eng 2013;18(12):1383–96.
[38] Popov EP, Amin NR, Louie JC, Stephen RM. Cyclic behavior of large beam-column assemblies. Eng J 1986;23(1):9–23.
[39] Morrison M, Schweizer D, Quayyum S, Hassan T. Experimental validation of an improved eight bolt unreinforced extended end-plate moment connection. J Struct Eng 2014 [submitted for publication].
[40] Morrison M, Schweizer D, Hassan T. Seismic enhancement of welded unreinforced flange-bolted web moment connections, Part 2: Experimental validation. J Struct Eng 2014 [submitted for publication].
[41] SAC Joint Venture. Strength and ductility of FR welded-bolted connections. Rep. No. SAC/BD-98/01; 1998.